Thermodynamics and Separation Process for Quaternary Acrylic Systems

Cuncun Zuo, Yaping Li, Chunshan Li, Shasha Cao, Haoyu Yao, and Suojiang Zhang
Beijing Key Laboratory of Ionic Liquids Clean Process, State Key Laboratory of Multiphase Complex Systems, Institute of Process Engineering, Chinese Academy of Sciences, Haidian District, Beijing 100190, P.R. China

DOI 10.1002/aic.15015
Published online September 7, 2015 in Wiley Online Library (wileyonlinelibrary.com)

Vapor-liquid equilibrium (VLE) and liquid-liquid equilibrium (LLE) data of binary and ternary acrylic systems were systematically measured. Subsequently, VLLE phase diagrams of binary systems, tridimensional VLE phase diagrams of methyl acrylate (MA)-methanol (Me)-H_2O ternary system, and quaternary LLE phase diagrams of MA-Me-H_2O-methyl acetate (MeOAc) system were constructed. These diagrams clearly demonstrated the effects of temperature on phase equilibrium. The experimental data was fitted by the NRTL and UNIQUAC models, and the best-fitted parameters were used to predict interaction properties of ternary and quaternary mixture. Therefore, the phase equilibrium data were provided as reference for the design of acrylic systems rectification or extraction process. Residue curve was mapped out for MA-Me-H_2O system through Aspen plus software. Finally, using thermodynamics and residue curve as theoretical basis, two novel separation processes were proposed and applied to the quaternary acrylic systems. © 2015 American Institute of Chemical Engineers *AIChE J*, 62: 228–240, 2016

Keywords: methyl acrylate, tridimensional VLE phase diagrams, quaternary LLE phase diagrams, thermodynamics, separation

Introduction

Methyl acrylate (MA), as an important industrial monomer, is extensively used to produce such materials as acrylic plastics and paints. The MA production route through propylene or propane oxidation has facilitated industrialization,[1–4] but the raw materials are mainly obtained from petroleum products. Recently, a new technology has been developed for MA production using MeOAc and formaldehyde as raw materials. To separate and purify MA, interaction parameters between MA and other by-products as well as residual materials are very essential.[5–8] Equilibrium thermodynamics has traditionally been treated separately in chemical engineering.[9]

The complexity of the separation of MA product systems is embodied in approximate boiling points and azeotropy, and problems also exist in other azeotropic systems.[10–12] Studies on the field have caused extensive research[13,14] and a method to locate binary mixture azeotropes was developed. Moreover, binary mixtures such as H_2O-MeOAc, H_2O-Me, Me-MeOAc, Me-MA, and MeOAc-MA have been reported in many literatures,[15–17] and the methods were evaluated by the comparison of the phase experimental data of azeotropic systems and calculated value. In recent years, according to the knowledge of previous researchers on approximate boiling points and azeotropic mixtures, the phase equilibrium and separation method of multivariate components have attracted the attention of numerous research.[18,19] Rodriguez-Donis et al.[20] extended the analysis to ternary systems, given that these systems could be easily visualized. Rooks et al.[21] also attempted to study approximate boiling points and azeotropic systems with more than three components, and several available methods were summarized in details. Among these MA synthesis systems, two ternary mixtures of H_2O-Me-MeOAc and Me-MeOAc-MA have been studied previously.[22–24] However, the results of previous researches are insufficient for other more complicated systems. It is essential to obtain the thermodynamics and separation process of multicomponent systems from phase equilibrium data. For a system with two or more phases at certain temperature and pressure, the equilibrium concentrations of all the components in all the phases are required. Thermodynamics provides a tool to meet this requirement. Phase equilibrium data containing VLLE and liquid-liquid equilibrium (LLE) data, are fundamentally essential to the analysis and design of the industrial separation processes.[25] In a series of distillation systems, vapor-liquid-liquid multiphase coexistence may occur because of the existence of the partially miscible components in mixtures, such as water and esters.[26]

This study aims to investigate the multiphase coexistence behavior of liquid mixtures which consist of MA, Me, MeOAc, and H_2O. Isobaric VLLE data of a binary system of H_2O-MA are systematically measured. Moreover, LLE data of two ternary systems of H_2O-Me-MA and H_2O-MeOAc-MA are presented at 303.15K, and tridimensional Vapor-liquid equilibrium (VLE) phase diagrams of H_2O-MA-Me ternary system and LLE phase diagrams of H_2O-MA-MeOAc-Me

Additional Supporting Information may be found in the online version of this article.

Correspondence concerning this article should be addressed to C. Li at csli@ipe.ac.cn or S. Zhang at sjzhang@ipe.ac.cn.

Table 1. Experimental Vapor Pressure Data and Antoine's Equation Constants of MA

Experimental data	1	2	3	4
$\ln(P^{sat})$/KPa	1.305083	2.239901	3.580737	4.628354
T/K	273.2700	293.8800	323.5800	352.9600
Parameters	A	B	C	$R^{\wedge}2$
Regression values	8.491001	734.9625	101.9991	0.9921541

quaternary system are successfully constructed, which could intuitively exhibit the effects of temperature on phase equilibrium. Based on the simulation calculation, two separation processes are proposed and designed, and the optimum results are proved to be available.

Experimental

Materials

The chemicals were purchased from Sinopharm Chemical Reagent Co. The purity of all the chemicals was checked via gas chromatography; the chemicals used were as follows: Me: 99.9% anhydrous; MeOAc: 99.5% anhydrous; and MA: 99.5% anhydrous inhibited with 100 ppm hydroquinone monomethyl ether. Distilled water was used in all the experiments.

Apparatus and procedure

The LLE still and improved Rose-Williams still for the VLLE measurement were provided by Zhejiang University, and the VLLE still was produced with a provision for both vapor and liquid recirculation. Figure 1 is the schematic diagram of the experimental apparatus. The VLLE temperature was measured using a mercury thermometer with an accuracy of ± 0.1 K, and the LLE temperature was maintained within ± 0.5 K via super-heated water bath.

To get Antoine's equation constants of MA, pure MA was injected into the Rose-Williams still and heated to boiling. When the status was stable, the pressure and temperature were recorded at the same time. Repeat the above procedures when the pressure was changed by vacuum pump.

The different proportions of H_2O and MA mixtures were injected into the VLE still separately, although this injection may be a separate phase. After 2 h of constant boiling, the vapor and liquid phases were sampled, while the mixture temperature and real-time atmospheric pressure were read. In addition, the LLE data for ternary systems of different composition, namely, H_2O-Me-MA and H_2O-MeOAc-MA, were measured using LLE glass still. Finally, the LLE data of the quaternary systems were also investigated using the equipment.

The samples were analyzed via gas chromatography (GC-2010 Plus, SHIMADZU) with barrier discharge ionization detector (BID).

Because the binary interaction parameters of MA-H_2O could not be found in the database of Aspen Plus, the VLLE data were fitted with Aspen to complement the binary interaction parameters. And separation processes of binary systems, ternary systems, and quaternary systems were simulated and optimized.

Results and Discussion

Table 1 shows the experimental vapor pressure data of MA. Pure component vapor pressure is calculated using Antoine's equation, as follows[27]

$$\ln(P^{sat}) = A - \frac{B}{(T - 273.15) + C} \tag{1}$$

where T is in Kelvin, and the constants A, B, and C are obtained by fitting the experimental vapor pressure data via nonlinear regression using the Polymath software.[28]

Vapor-Liquid-Liquid Equilibrium of MA-H_2O System

A binary mixture MA-H_2O was chosen as the initial solution to investigate VLLE for the ternary subsystems and quaternary subsystems mentioned in the present study. The experiment and calculated VLLE data for MA-H_2O binary system are listed in

Table 2. Experimental VLE Data and Calculated Data for MA(1) and H_2O(2) Using the NRTL and UNIQUAC Models

T/K			VLE					
T^{Exp}	T^{Est}_{NRTL}	T^{Est}_{UNIQ}	x_1^{Exp}	$x_1^{Est\text{-}N}$	$x_1^{Est\text{-}U}$	y_1^{Exp}	$y_1^{Est\text{-}N}$	$y_1^{Est\text{-}U}$
352.36	353.16	353.16	1.0000	1.0000	1.0000	1.0000	1.0000	1.0000
349.07	347.84	347.21	0.98090	0.98100	0.98100	0.90990	0.82210	0.80480
346.95	346.28	345.74	0.97220	0.97230	0.97230	0.85640	0.77580	0.76230
345.35	343.87	343.70	0.95010	0.95020	0.95020	0.80800	0.70290	0.70180
344.65	343.63	343.51	0.94740	0.94750	0.94750	0.77540	0.69680	0.69710
344.37	341.48	342.16	0.78990	0.78980	0.78980	0.72560	0.62950	0.65510
344.58	338.74	340.34	0.18650	0.18640	0.18650	0.65900	0.76870	0.74640
347.36	339.52	340.84	0.14680	0.14630	0.14650	0.61490	0.76090	0.74190
350.25	340.34	341.41	0.12820	0.12740	0.12780	0.58280	0.75250	0.73640
351.25	340.84	341.76	0.11890	0.11800	0.11840	0.57250	0.74670	0.73240
352.65	341.67	342.33	0.10670	0.10570	0.10610	0.56150	0.73680	0.72560
354.45	342.69	343.06	0.095400	0.094300	0.094700	0.53360	0.72440	0.71680
355.95	344.55	344.42	0.078600	0.077600	0.077800	0.50910	0.69890	0.69830
357.35	346.29	345.75	0.067100	0.066100	0.066300	0.47130	0.67350	0.67930
358.45	349.34	348.20	0.051300	0.050600	0.050700	0.45310	0.62310	0.64010
360.65	352.23	350.68	0.040700	0.040200	0.040200	0.40040	0.57160	0.59850
362.15	354.87	353.06	0.032700	0.032300	0.032300	0.35590	0.51890	0.55420
363.65	359.33	357.34	0.021600	0.021500	0.021400	0.31220	0.41540	0.46180
365.16	361.86	359.94	0.016600	0.016500	0.016500	0.25300	0.35070	0.40010
369.25	370.58	370.03	0.0026000	0.0026000	0.0026000	0.10320	0.074300	0.095200
373.00	372.81	372.81	0	0	0	0	0	0

Table 3. Experimental LLE and Calculated Data for MA(1) and H_2O(2) Using the NRTL and UNIQUAC Models

T/K			LLE					
T^{Exp}	T^{Est}_{NRTL}	T^{Est}_{UNIQ}	$x_1^{I\text{-}Exp}$	$x_1^{I\text{-}Est\text{-}N}$	$x_1^{I\text{-}Est\text{-}U}$	$x_1^{II\text{-}Exp}$	$x_1^{II\text{-}Est\text{-}N}$	$x_1^{II\text{-}Est\text{-}U}$
300.65	300.74	300.71	0.04242	0.04050	0.04096	0.9471	0.95268	0.95260
308.15	308.16	308.16	0.04571	0.04563	0.04561	0.9497	0.95218	0.95217
313.15	313.16	313.17	0.04969	0.04931	0.04903	0.9520	0.95180	0.95182
318.15	318.12	318.13	0.05231	0.05315	0.05266	0.9535	0.95137	0.95141
323.15	323.10	323.12	0.05616	0.05720	0.05657	0.9555	0.95090	0.95096
330.65	330.57	330.58	0.06126	0.06361	0.06300	0.9560	0.95014	0.95019
333.15	333.08	333.10	0.06491	0.06587	0.06534	0.9584	0.94986	0.94990
338.15	338.09	338.09	0.06801	0.07051	0.07027	0.9512	0.94928	0.94929
341.15	341.14	341.14	0.07135	0.07343	0.07349	0.9415	0.94891	0.94890
344.35	344.36	344.35	0.07444	0.07659	0.07705	0.9379	0.94851	0.94846

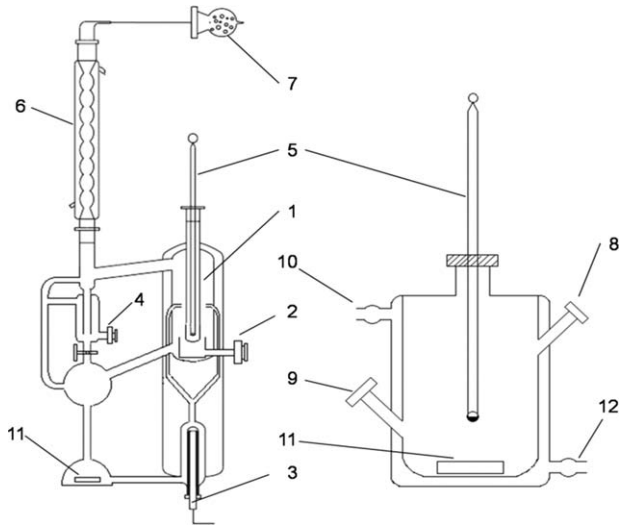

Figure 1. Schematic diagrams of the VLLE still and LLE cell: 1, equilibrium chamber; 2, liquid-phase sampling point; 3, heating rod; 4, vapor-phase sampling point; 5, thermometer; 6, condenser; 7, desiccator; 8, 9-sampling point; 10, 12-outlet and inlet of thermostatic water; 11, magnetic stirrer.

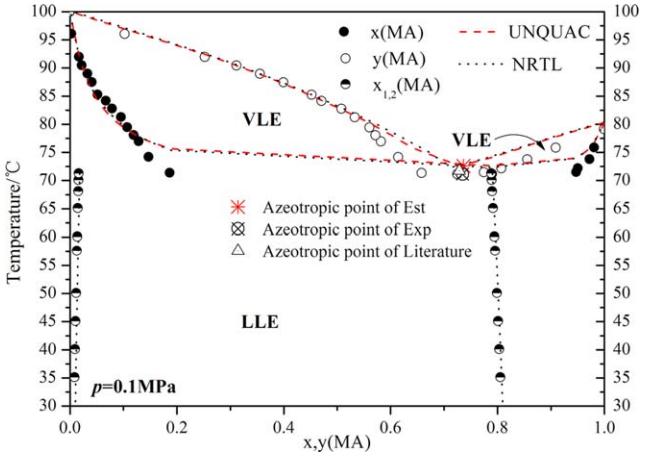

Figure 2. Experiment VLLE data and calculated MA-H_2O data using the NRTL and UNIQUAC models.

[Color figure can be viewed in the online issue, which is available at wileyonlinelibrary.com.]

Table 4. Deviations between the Calculated and Experimental Values on x_1, y_1, and T through the NRTL and UNIQUAC Models for MA(1) and H_2O(2)

Model	AAD(x_1)[b]	AAD(T)[b]	AAD(y_1)[b]
VLE for MA(1)+H_2O(2)			
NRTL	0.0023	0.0328	0.00090
UNIQUAC	0.0033	0.0346	0.0013
LLE for MA(1)+H_2O(2)			
NRTL	0.0027	0.00560	–
UNIQUAC	0.0027	0.00540	–

[b] $AAD(y)=(1/N)\sum_{i=1}^{N}|y_i^{exp}-y_i^{cal}|$; [b] $AAD(T)=(1/N)\sum_{i=1}^{N}|T_i^{exp}-T_i^{cal}|$; [b] $AAD(x)=(1/N),\sum_{i=1}^{N}|x_i^{exp}-x_i^{cal}|$.

Tables 2 and 3, respectively, and also plotted in Figure 2. In addition to the presence of two liquid phases, MA forms a minimum-boiling azeotrope with H_2O at 344.2 K with a mole fraction of MA as 0.728. Reshtov et al.[29] investigated the azeotropic phenomenon of acrylate systems, and he considered the effects of different pressures and the carbon number of long-stain on azeotropic points. However, complete VLE data of MA-H_2O binary system could not be found in previous literatures, and also Aspen database. Several experimental data points exist with overall (combined) liquid compositions ranging from 0 to 1. Each of these compositions provides a H_2O-rich liquid phase of mole fraction of MA and a MA-rich liquid phase of mole fraction of MA in different equal quantities.

The Aspen Plus V7.3 (Aspen Tech) process simulation software is used to fit the experimental VLLE data via NRTL and UNIQUAC equations, assuming that the vapor is an ideal gas (a reasonable assumption at 1 atm). The NRTL and UNIQUAC equilibrium equations are used to fit the experiment data and to calculate the activity coefficients of components and the calculated activity coefficients are used to estimate phase equilibrium data by Eq. 2. Vapor pressures of MA in Eq. 2 are obtained from the experimentally determined Antoine's equation coefficients in Table 1. The pure component parameters of the NRTL and UNIQUAC models are generated through Aspen Plus V7.3.

Table 5. Binary Interaction Parameters of the NRTL Model for H_2O(1), MA(2), MeOAc(3), and Me(4)

i-j	α_{ij}	a_{ij}	b_{ij}	a_{ji}	b_{ji}
1-2	0.3	−1.63346	1225.66	2.55419	−78.8107
1-3	0.3	3.52970	−308.957	−2.91120	1240.36
1-4	0.3	4.82410	−1329.54	−2.62600	828.387
2-3	0.3	−0.0323475	−24.5139	−0.898347	340.784
2-4	0.3	−1.60344	729.116	0.591666	0
3-4	0.3	0	234.866	0	130.505

Table 6. Binary Interaction Parameters of the UNIQUAC Model for H_2O(1), MA(2), MeOAc(3), and Me(4)

i-j	a_{ij}	b_{ij}	a_{ji}	b_{ji}
1-2	1.186981	−337.6946	−3.932800	456.4566
1-3	−1.918700	525.7553	3.328600	−1341.769
1-4	0.6437000	−322.1312	−1.066200	432.8785
2-3	−0.8248288	71.09680	1.075714	−207.1669
2-4	0.5348617	−541.9107	0.08483421	28.75961
3-4	0	−337.4185	0	54.3901

$$y_i = \gamma_i^{\mathrm{I}} x_i^{\mathrm{I}} P_i^{\mathrm{sat}} = \gamma_i^{\mathrm{II}} x_i^{\mathrm{II}} P_i^{\mathrm{sat}} \tag{2}$$

The experimental VLLE datasets on both ternary and quaternary systems have been compared with the calculated data using the NRTL and UNIQUAC models, which can describe partial miscibility.[30] The NRTL model developed by Renon and Prausnitz[31] was selected to correlate the experimental results. Liu et al.,[32] Topphoff et al.,[33] Kato et al.,[34] and Doker et al.[35] also applied the NRTL equation to correlate the VLLE data of systems that contain ILs. The NRTL equations in the present study for the activity coefficients in the solution of n components are shown in the following

$$\ln \gamma_i = \frac{\sum_{j=1}^{c} \tau_{ji} G_{ji} x_j}{\sum_{k=1}^{c} G_{ki} x_k} + \sum_{j=1}^{c} \frac{x_j G_{ij}}{\sum_{k=1}^{c} G_{ki} x_k} \left[\tau_{ij} - \left(\sum_{r=1}^{c} x_r \tau_{rj} G_{rj} / \sum_{k=1}^{c} G_{ki} x_k \right) \right] \tag{3}$$

$$G_{\mathrm{ij}} = \exp(-\alpha_{\mathrm{ij}} \tau_{\mathrm{ij}}),\ G_{ji} = \exp(-\alpha_{ij} \tau_{ji}),$$

$$\tau_{ij} = a_{ij} + b_{ij}/T,\ \tau_{ij} \neq \tau_{ji},\ \tau_{ii} = \tau_{jj} = 0,\ \alpha_{ij} = \alpha_{ji}.$$

where T is the absolute temperature K, and a_{ij} and b_{ij} are the NRTL binary interaction parameters.

The UNIQUAC model developed by Anderson and Prausnitz[36] is used to fit the experimental VLLE data. The multicomponent expressions for the activity coefficient of the UNIQUAC equations are expressed by

$$\ln \gamma_i = \ln \frac{\phi_i}{x_i} + \frac{z}{2} q_i \ln \frac{\theta_i}{\phi_i} + l_i - \frac{\phi_i}{x_i} \sum_{j=1}^{nc} x_j l_j + q_i' \left[1 - \ln \left(\sum_{j=1}^{nc} \theta_j' \tau_{ji} \right) - \sum_{j=1}^{nc} \frac{\theta_j' \tau_{ji}}{\sum_{k=1}^{nc} \theta_k' \tau_{ji}} \right] \tag{4}$$

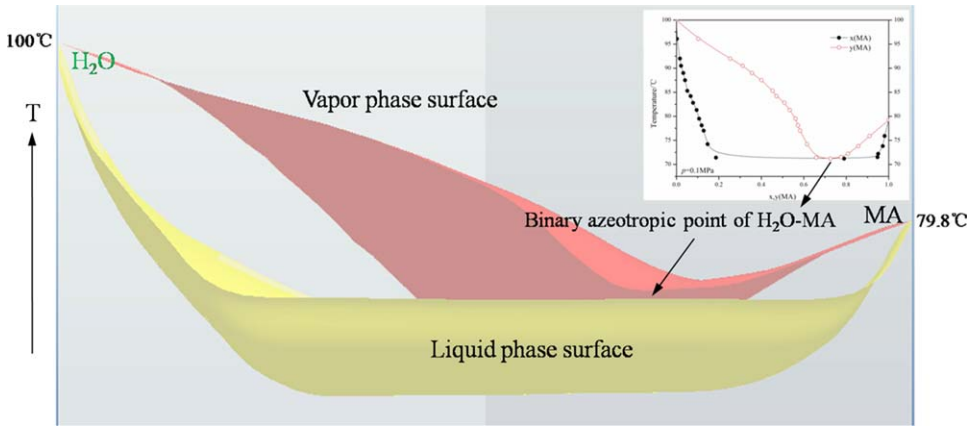

Figure 3. VLE phase diagram of MA-H_2O binary system and tridimensional VLE diagram of H_2O-MA-Me ternary system.

[Color figure can be viewed in the online issue, which is available at wileyonlinelibrary.com.]

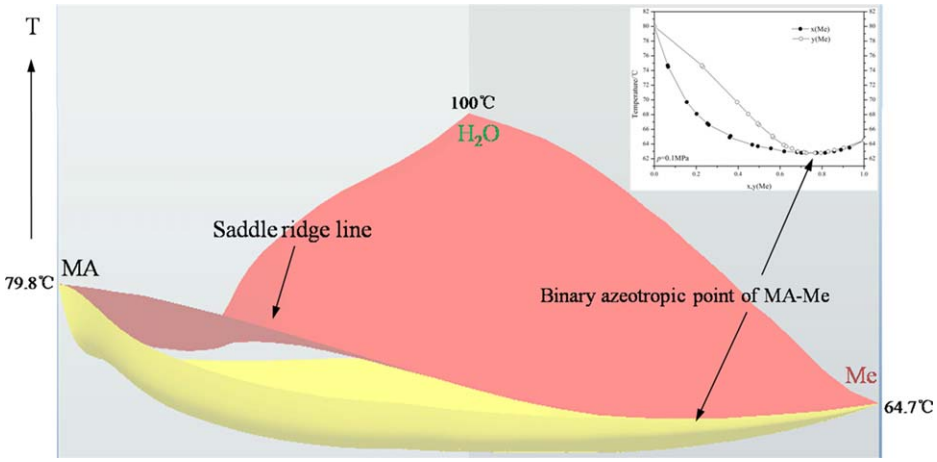

Figure 4. VLE phase diagram of MA-Me binary system and tridimensional VLE diagram of H_2O-MA-Me ternary system.

[Color figure can be viewed in the online issue, which is available at wileyonlinelibrary.com.]

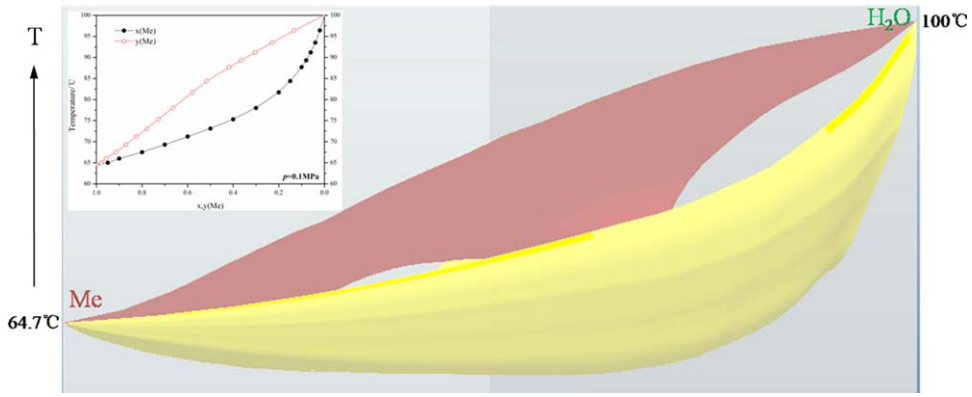

Figure 5. VLE phase diagram of Me-H_2O binary system and tridimensional VLE diagram of H_2O-MA-Me ternary system.

[Color figure can be viewed in the online issue, which is available at wileyonlinelibrary.com.]

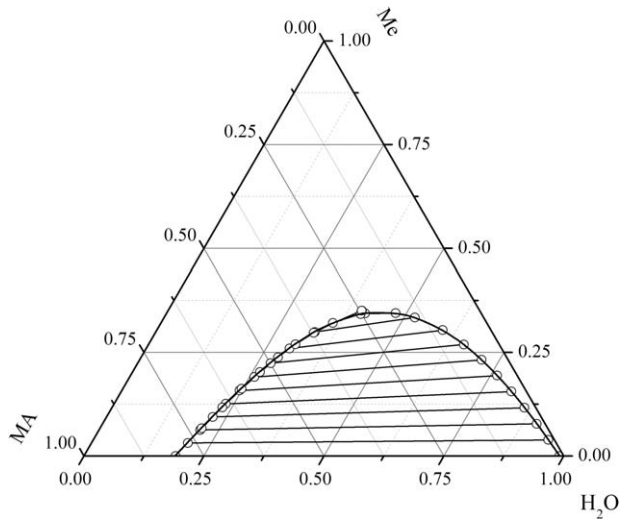

Figure 6. LLE phase diagram of MA-Me-H_2O ternary system.

$$\phi_i=\frac{r_i x_i}{\sum_{k=1}^{nc} r_k x_k},\ \theta_i=\frac{q_i x_i}{\sum_{k=1}^{nc} q_k x_k},\ \theta'_i=\frac{q'_i x_i}{\sum_{k=1}^{nc} q'_k x_k}.$$

$$\tau_{ij}=\exp\left(a_{ij}+\frac{b_{ij}}{T}\right),\ l_i=\frac{z}{2}(r_i-q_i)-(r_i-1),\ \text{and}\ z=10.$$

where T is the absolute temperature K; and a_{ij} and b_{ij} are the UNIQUAC binary interaction parameters.

Binary interaction parameters obtained from the NRTL and UNIQUAC models are shown in Tables 5 and 6.

The experimental data were entered into Aspen Plus v7.3 as T-x-y and T-x-x sets. Data regression was then performed simultaneously with both datasets to calculate each binary interaction parameter τ_{ij} and τ_{ji} using Eqs. 3 and 4. The binary interaction parameters are regressed from the experimental data using the least square method.[37–39]

Compared with the UNIQUAC model, the predicted VLLE data from the NRTL model describe the experimental data better for the binary MA-H_2O system. The deviations were shown in Table 4. The azeotropic compositions and temperature, and the vapor-liquid region are described exceptionally well; the liquid-liquid phase region is described reasonably for both

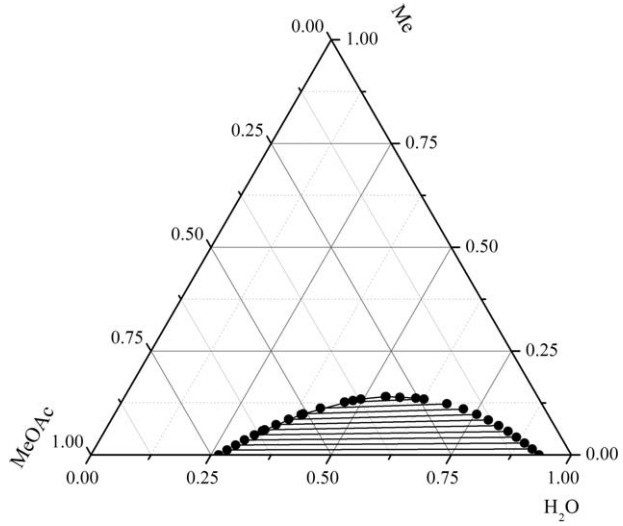

Figure 7. LLE phase diagram of Me-H_2O-MeOAc ternary system.

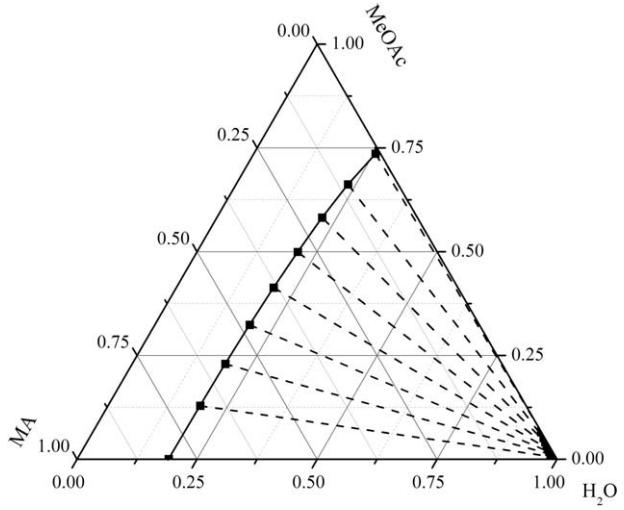

Figure 8. LLE phase diagram of MA-H_2O-MeOAc ternary system.

Table 7. Experimental LLE Data for the Quaternary System of H_2O(1), MA(2), and MeOAc(3), for the Mole Fractions x at 303.15 K and Atmospheric Pressure

	H_2O phase(I)			Organic phase(II)		
T/K	x_1^I	x_2^I	x_3^I	x_1^{II}	x_2^{II}	x_3^{II}
303.15	0.93372	0	0.06628	0.25688	0	0.74312
303.15	0.93515	0.000285	0.06456	0.25411	0.0099200	0.73596
303.15	0.94671	0.00246	0.05083	0.23356	0.10456	0.66188
303.15	0.95563	0.00399	0.04038	0.21998	0.19784	0.58218
303.15	0.96302	0.00518	0.03180	0.21045	0.29040	0.49915
303.15	0.96942	0.00615	0.02443	0.20355	0.38334	0.41311
303.15	0.97515	0.00698	0.01786	0.19853	0.47797	0.32351
303.15	0.98042	0.00772	0.01186	0.19496	0.57578	0.22926
303.15	0.98535	0.00839	0.006260	0.19261	0.67847	0.12893
303.15	0.99088	0.00912	0	0.19128	0.80872	0

Table 8. Experimental LLE Data for the Quaternary System of H_2O(1), MA(2), and Me(3) for Mole Fractions x at 303.15 K and Atmospheric Pressure

	H_2O phase(I)			Organic phase(II)		
T/K	x_1^I	x_2^I	x_4^I	x_1^{II}	x_2^{II}	x_4^{II}
303.15	0.99088	0.009120	0	0.19128	0.80872	0
303.15	0.94866	0.01268	0.03866	0.20085	0.76764	0.03151
303.15	0.90513	0.01735	0.07752	0.21089	0.72621	0.06291
303.15	0.8601	0.02343	0.1165	0.22154	0.68416	0.09430
303.15	0.8133	0.03134	0.1554	0.23304	0.64113	0.1258
303.15	0.76437	0.04167	0.1940	0.24571	0.59658	0.1577
303.15	0.71273	0.05535	0.2319	0.26008	0.54969	0.1902
303.15	0.65739	0.07389	0.2687	0.27716	0.49899	0.2239
303.15	0.59625	0.1003	0.3034	0.29903	0.44155	0.25949
303.15	0.52297	0.1431	0.3340	0.33204	0.36897	0.2990

H_2O-rich and MA-rich phases. These parameters are reported in Tables 5 and 6.

VLE and LLE of Ternary (H_2O-MA-Me) and Quaternary System (H_2O-MA-MeOAc-Me)

To predict the ternary VLE H_2O-MA-Me, a set of VLLE data of binary H_2O-MA were obtained through the experiments. As illustrated in Figure 2, the fitted data by the NRTL and UNIQUAC models agree well with the experimental data, that is, the regression parameters are reasonable and satisfactory. Figures 3–5 demonstrate binary VLE phase diagrams and ternary tridimensional VLE diagrams. The painting method and interpretation of these figures were mentioned in the Supporting information. MA could form binary minimum azeotropes with H_2O and Me, and the azeotropic phenomenon

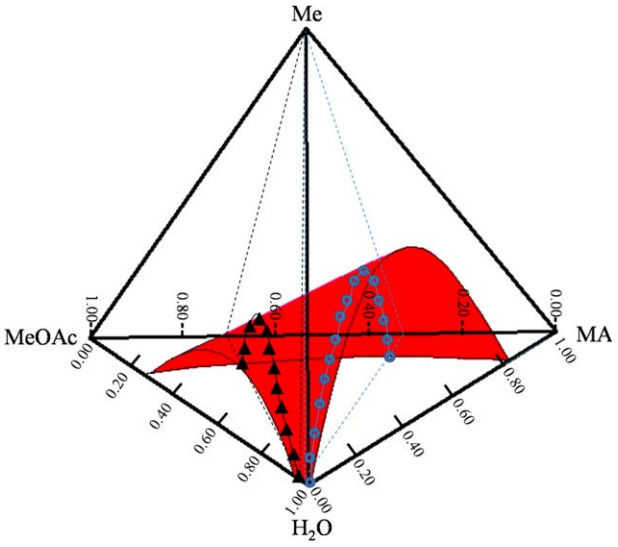

Figure 9. Quaternary LLE phase diagram of MA-Me-H_2O-MeOAc system.

[Color figure can be viewed in the online issue, which is available at wileyonlinelibrary.com.]

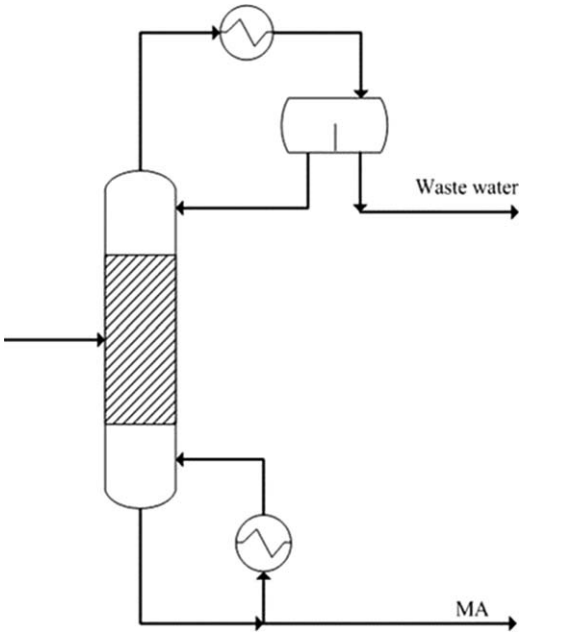

Figure 10. Schematic diagram of MA-H_2O binary system.

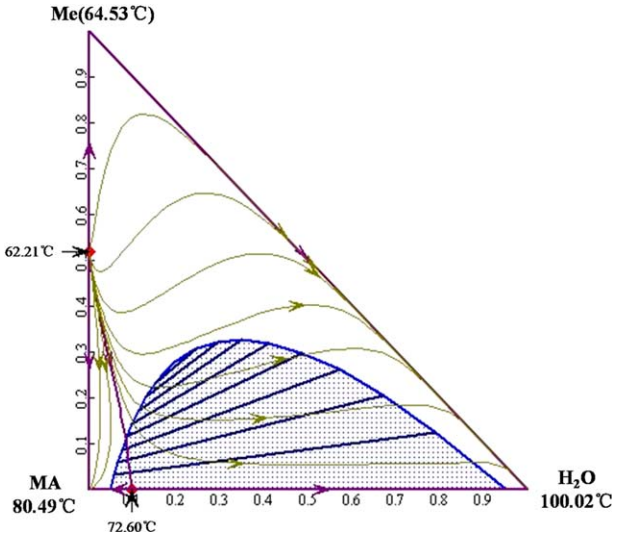

Figure 11. Residual curve of the H_2O-MA-Me ternary system.

[Color figure can be viewed in the online issue, which is available at wileyonlinelibrary.com.]

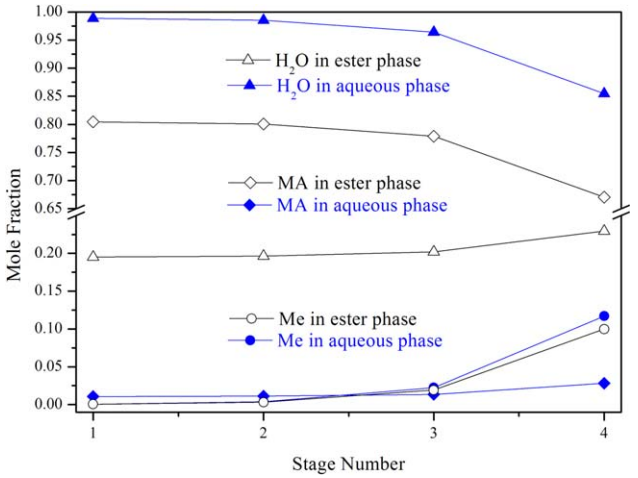

Figure 13. Composition distribution on each theoretical plate of the extraction column in process I.

[Color figure can be viewed in the online issue, which is available at wileyonlinelibrary.com.]

does not exist between H_2O and Me binary mixture. Wherein, two azeotropic points fall on the saddle surface of ternary tridimensional diagrams. Figure 4 visually shows that the vapor and liquid surfaces are almost overlapping in areas of high methanol concentration. In other words, there are ternary azeotrope phenomenon among MA, Me, and H_2O mixture in this area, especially under appropriate pressure circumstance, which is consistent with the azeotrope research of MA-Me-H_2O ternary system in previous literature.[29]

Although the thermodynamic models generate excellent correlations with the experimental data, the deviations of binary systems are slightly larger than that of ternary systems. The result is because that Aspen Plus simulator uses the binary interaction parameters to obtain the interaction parameters of ternary systems, and predict the VLLE of ternary systems. This approach increases the deviations of the prediction of the ternary VLLE compared with the binary deviations.

According to results reported in literature,[30] none of the parameters obtained through the VLE correlation seems to provide very satisfactory liquid boiling envelope predictions in most systems. And, the parameters obtained through the LLE correlation cannot predict the vapor phase composition accurately. Nevertheless, the experimental VLLE data are fitted by the NRTL and UNIQUAC models in our study, and the better one is used to obtain model parameters. Afterwards, these parameters are used to estimate the VLLE data.

The experimental and correlated LLE data of H_2O-Me-MA are listed in Tables 7 and 8. To provide a valid theoretical basis for the separation of MA-Me-H_2O-MeOAc quaternary acrylic system, we further build quaternary LLE phase diagram. Figures 6–8 are the ternary phase diagram of MA-Me-H_2O, Me-H_2O-MeOAc, and MA-H_2O-MeOAc system at a temperature of 303.15 K, respectively. According to the above three pictures, the quaternary VLE phase diagram of MA-Me-H_2O-MeOAc system was successfully constructed, as illustrated in Figure 9. In accordance with the LLE phase diagram,

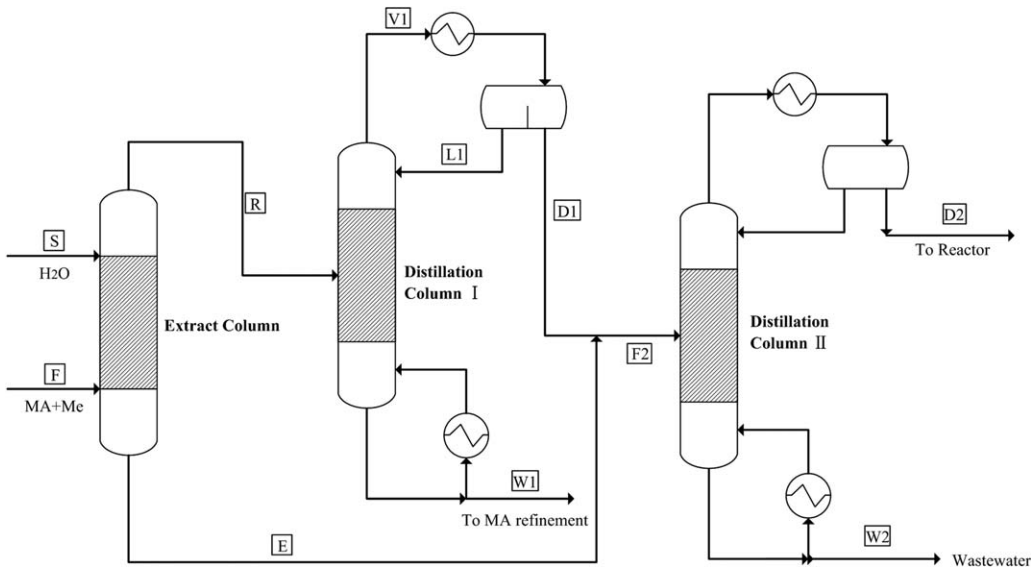

Figure 12. Separation process I of the H_2O-MA-Me ternary system.

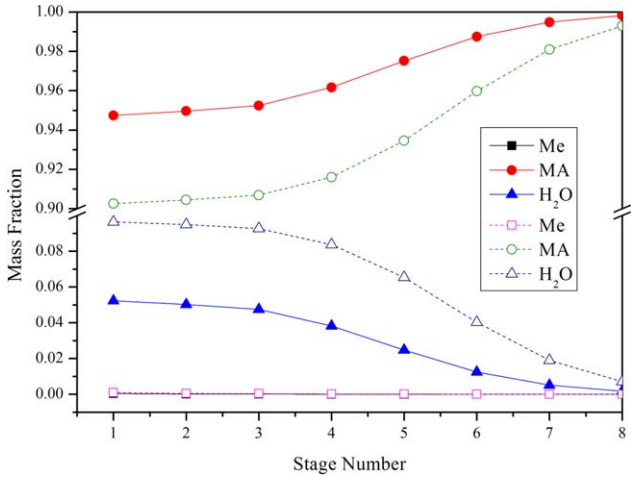

Figure 14. Composition distribution on each theoretical plate of the first distillation column in process I.

[Color figure can be viewed in the online issue, which is available at wileyonlinelibrary.com.]

H_2O-MA is the only pair that is partially miscible, whereas the two liquid pairs of H_2O-Me and Me-MA are completely miscible.

The NRTL model is used to correlate the experimental data for the ternary mixture reported here. The calculation tie-lines in Figures 6–8 were obtained using the NRTL equation, and these tie-lines well agree with the experimental data. The optimum NRTL interaction parameters a_{ij} between H_2O, Me, and MA are determined using the observed LLE data, where the interaction parameters describe the interaction energy between each pair of compounds.

Figures 6–8 demonstrate both the experimental and calculated LLE data of three subsystems of H_2O-MA-Me-MeOAc quaternary system. The root-mean-square deviations between the calculated and measured values for x_{11}, x_{21}, x_{12}, and x_{22} are 0.0028, 0.0019, 0.0042, and 0.0012, respectively. The LLE data of H_2O-MA-Me at 303.15 K are calculated using the

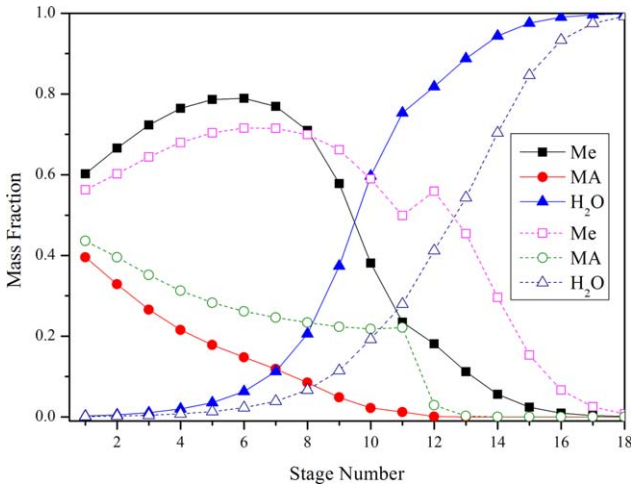

Figure 15. Composition distribution on each theoretical plate of the second distillation column in process I.

[Color figure can be viewed in the online issue, which is available at wileyonlinelibrary.com.]

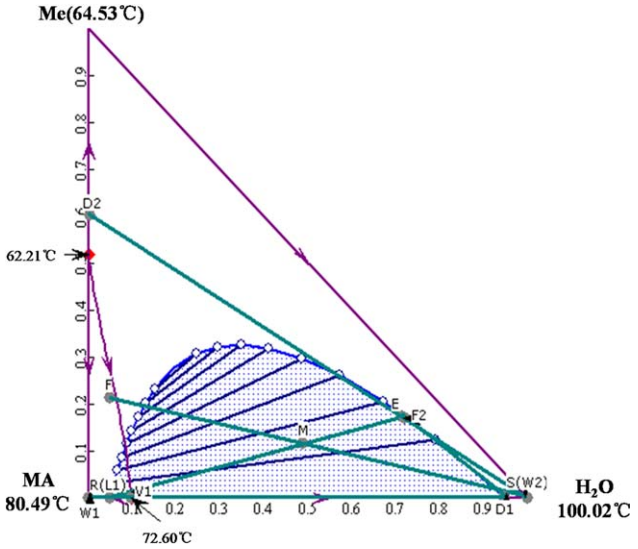

Figure 16. Material balance lines for separation from a mixture of H_2O-MA-Me in process I.

[Color figure can be viewed in the online issue, which is available at wileyonlinelibrary.com.]

NRTL equation, and the results are shown in Figures 6–8. To clearly present the binodal curve in the form of the surface, a composition tetrahedron was constructed (Figure 9). The intersections of the three edges and the Tri-prism horizontal section represent pure MA, H_2O, and Me, respectively, and the ordinate represents temperature.

Applications in the Separation Process Design

According to Figure 2, as there is azeotropic point in MA-H_2O binary system, one pure component and a minimum azeotrope could be obtained at the top and the bottom through a simple distillation. But when the azeotrope was cooled down via a condenser, the mixture was divided into two phases in a decantation and the component of ester phase can successfully span across the azeotropic point. This separation method can be realized as the separation approach of binary system containing binary azeotrope. Ester phase reflows and water phase dischargs from the top, high-purity MA can be obtained at the bottom. In Figure 10, the column was called dehydration column of MA and a schematic diagram of MA-H_2O binary system was given.

Tridimensional diagrams of MA-Me-H_2O ternary system show there are two binary azeotropes in the ternary mixture. Additionally, the vapor and liquid surfaces are almost overlapping in area of high methanol concentration, which indicate it is difficult to separate three components through the conventional rectification process. Therefore, combining tridimensional diagrams with the residual curve (Figure 11), the rectification and extraction processes were used together to achieve the separation of ternary system. The extraction process was performed to continually reduce the methanol concentration of the ternary mixture, which could make the composition of ternary system stay away from the area of high methanol concentration. Therefore, in cooperation with extraction and rectification, the separation of ternary system could be realized.

The residual curve represents the remaining liquid composition changes over time in the single-stage batch distillation process. Thus, the residual curve is constructed to analyze the feasibility of the distillation process. Two minimum azeotropes

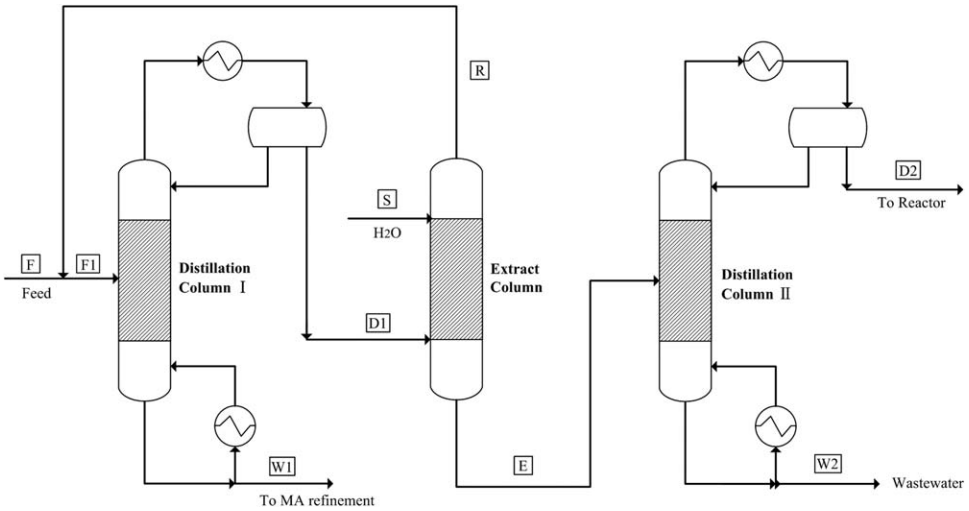

Figure 17. Separation process II of the H_2O-MA-Me ternary system.

exist in the MA-Me-H_2O ternary system are studied, namely, MA-Me homoazeotrope and MA-H_2O saddle homoazeotrope. The calculated residue curve of the mixture along with the binodal curve at $T = 303.15$ K is presented in Figure 11. In this ternary residual curve, two sets of binary azeotrope systems are evident. The azeotropic temperature of Me and MA azeotrope is 335.36 K, and the azeotropic temperature of H_2O and MA is 345.75 K. Five fixed points are found on the ternary phase diagram, that is, two azeotropic points and three vertices. The connecting line of the two azeotropic points is called distillation boundary line (purple line), and the residual curve neither intersects nor crosses the distillation boundary line. No matter where the feed location is, pure component cannot be obtained at the bottom and top of tower at the same time along the remaining curves. In this work, two separation ideas are proposed to obtain highly purified MA through a relatively simple process.

First, as can be seen from Figure 11, the distillation boundary map, binodal curve, and the horizontal edge of ternary phase equilibrium triangle intersect to form a small area. During the distillation, if the layered components could be timely

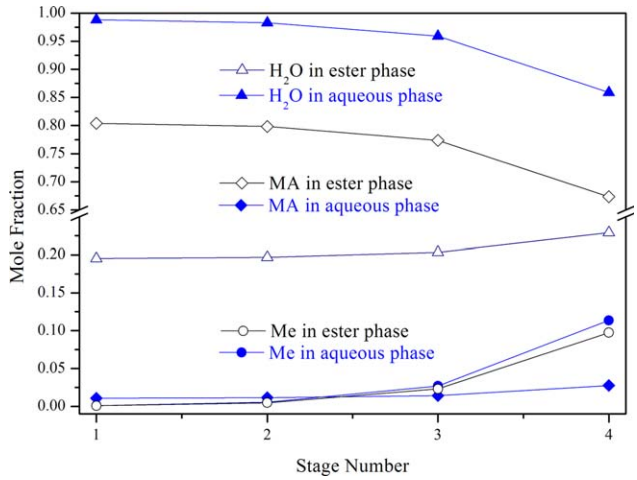

Figure 19. Composition distribution on each theoretical plate of the extraction column in process II.

[Color figure can be viewed in the online issue, which is available at wileyonlinelibrary.com.]

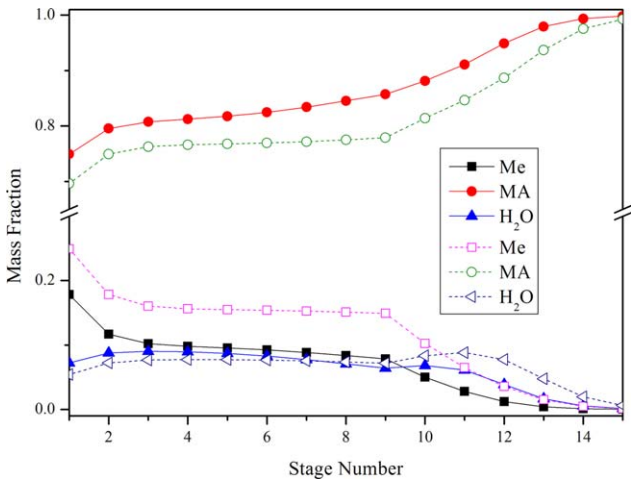

Figure 18. Composition distribution on each theoretical plate of the first distillation column in process II.

[Color figure can be viewed in the online issue, which is available at wileyonlinelibrary.com.]

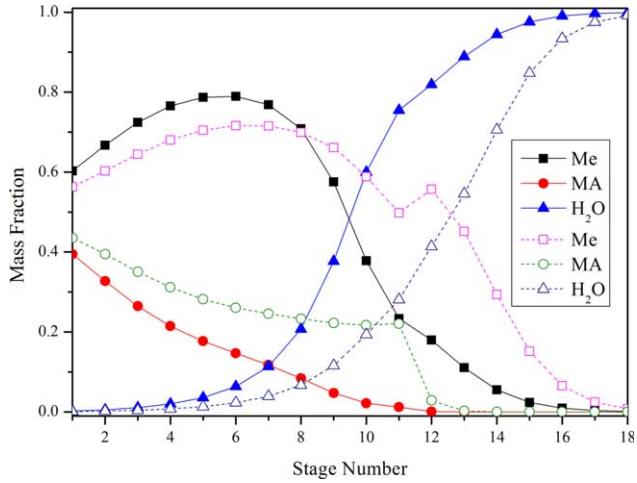

Figure 20. Composition distribution on each theoretical plate of the second distillation column in Process II.

[Color figure can be viewed in the online issue, which is available at wileyonlinelibrary.com.]

removed via decantation or extraction separation, the residual curve can successfully cross the distillation boundary line, and pure components are obtained at the bottom and at the top.

Second, the feed point (F) falls in the small area enclosed by the distillation boundary line and the sides of ternary phase diagram triangle. In contrast to the first process, the material is primitively fed into a distillation column. The composition distribution of the distillation column is shown in Figure 18, which displays that the pure MA product obtained at the bottom and the components from the top that entered into the extraction column.

Two separation process calculations are designed using the Aspen Plus software, and the results were shown in Figures 12 and 17, which demonstrate the schematic diagrams of processes I and II.

Process I comprises the following workflows. The extraction column is designed as the first column during the whole separation process. The crude MA mixture is fed in the bottom (F) of the extraction column and H_2O (S) is used as extraction agent at the top. When two liquid phases contact completely, Me is redistributed in both phases. The light components from the top exit (R) are the MA-rich phase and the heavy components from the bottom (E) are the H_2O phase that contains Me. The composition distribution on each theoretical plate of the extraction column is shown in Figure 13. In addition, the materials (R) fed into the distillation column I for H_2O removal, pure MA (W1) could be obtained at the bottom, and the composition at top of the column is about the azeotrope of H_2O and MA. Consistent with the results demonstrated in Figure 2, the azeotrope is divided into two phases after cooling in the whole condenser. Therefore, a decanter is setup at the top and the ester phase (L1) reflowed. The separation efficiency of the column is greatly improved. Figure 14 shows the composition distribution curve of the column. The third column is the distillation column II for water recycling. Waste water from the bottom (E) of the extraction column and the top (D1) of the distillation column I are mixed together to be separated. The relatively pure water (W2) obtained from the bottom can be recycled to the extraction column, and the mixture of Me and residual MA at the top (D2) of the column reflow back to the reactor of the MA production process. The composition distribution on each theoretical plate of the distillation column II is exhibited in Figure 15. Figure 16 shows the material balance lines for the separation of this process.

In contrast to process I, process II is characterized by the mixture (F) primarily fed into a distillation column before the extraction separation. The results demonstrate that some pure MA (W1) is obtained at the bottom of the column, and the components (D1) from the top of the tower entered the extraction column with water (S) as extraction agent. The raffinate phase (R) reflows back to the feed (F1) of the first distillation column and the extraction phase (E) is pumped into the distillation column II for water (W2) recycling. The D2 from the top returns back to the reactor of the MA production process. The composition distribution diagrams of the three columns are illustrated in Figures 18–20. Figure 21 shows the operation line of each tower.

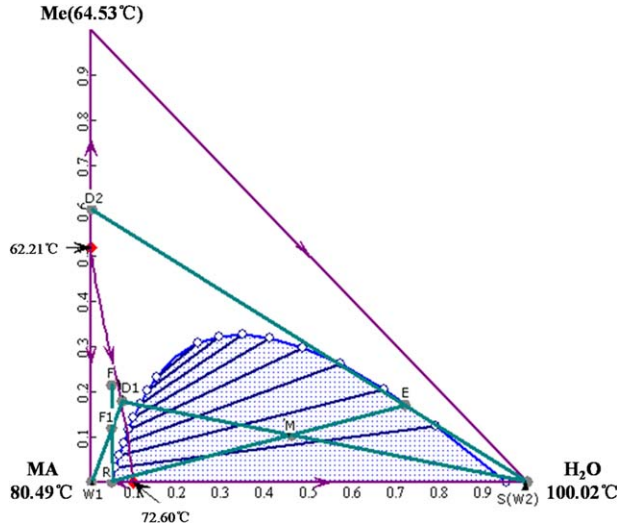

Figure 21. Material balance lines for separation from a mixture of H_2O-MA-Me in process II.

[Color figure can be viewed in the online issue, which is available at wileyonlinelibrary.com.]

Table 11. Comparison of Two Processes

	Total number of towers	No. of extraction columns	No. of distillation columns	Total load of condenser/ KW	Total load of reboiler/ KW
ProcessI	3	1	2	−169.8	208.61
ProcessII	3	1	2	−278.28	312.44

Table 9. Material Data of Each Point in Process I

	F	S	R	E	V1	L1	D1	W1	D2	W2
T/℃	40	40	38.9	44.1	72.5	40	40	79.9	62.3	99.8
MF (kg/h)	500	430	314.547	615.453	290	274.281	15.705	298.828	176.1	439.368
Me (wt %)	0.214	0	0.000191	0.174	0.001	0.001	0.004	482PPB	0.605	0.000972
MA (wt %)	0.737	0	0.952	0.112	0.902	0.951	0.05	0.999	0.393	0
H_2O (wt %)	0.049	1	0.048	0.714	0.097	0.049	0.946	0.001	0.002	0.999

MF: mass flow; PPB:10^{-9}.

Table 10. Material Data of Each Point in Process II

	F1	D1	W1	S	E	R	V2	D2	L2	W2	D3	W3
T/℃	40	65.1	80.4	40	55.4	39	72.5	40	40	79.6	62.2	99.8
MF (kg/h)	500	440	60	400	600.269	239.731	220	11.759	208.254	227.984	187.4	412.869
Me (wt %)	0.214	0.243	0.00033	0	0.178	0.000138	0.000723	0.003	0.001	0.000001	0.569	0.001
MA (wt %)	0.737	0.701	0.998	0	0.134	0.952	0.903	0.05	0.951	0.998	0.429	0
H_2O (wt %)	0.049	0.056	0.001	1	0.688	0.048	0.097	0.947	0.048	0.002	0.002	0.999

MF: mass flow

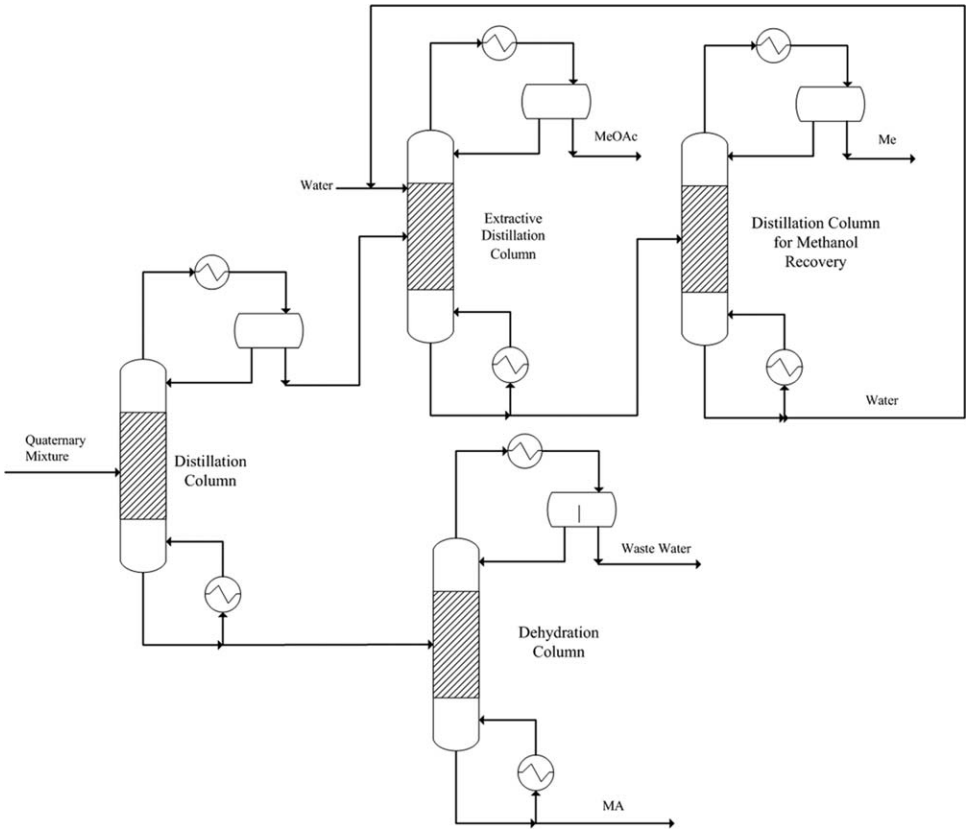

Figure 22. Flow chart for the separation process for the Me-MeOAc-H_2O-MA quaternary system.

As shown in Figures 11 and 12, the feed to be separated contains MA and Me, and the flow rate is 500 kg/h. The compositions of each point of the two processes are shown in Tables 9 and 10.

As can be clearly seen form Table 11, the comparison of these two processes shows the same number of extraction and distillation columns, but process I requires less energy for the condenser and reboiler than process II.

Based on the above ideas, the separation process for the Me-MeOAc-H_2O-MA quaternary system is established. Figure 22 shows the flow chart of the separation process for the Me-MeOAc-H_2O-MA quaternary system.

The first distillation column is used for MeOAc recycling. MeOAc is obtained at the top by the extractive distillation column and Me was recycled from the aqueous phase with a distillation column. Figures 25 and 26 demonstrate the composition distributions of the two columns. Figure 2 shows that the composition at the bottom is located in the two-phase region. Hence, a decanter is setup and the ester phase is further separated through the dehydration column to obtain MA. The

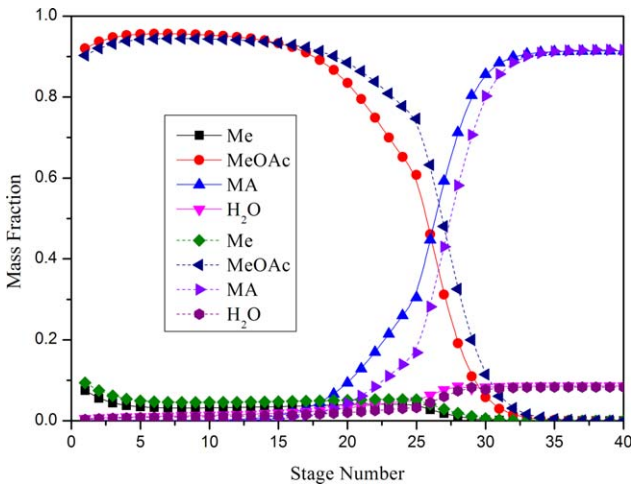

Figure 23. Composition distribution for the Me-MeOAc-H_2O-MA quaternary system in the first distillation column.

[Color figure can be viewed in the online issue, which is available at wileyonlinelibrary.com.]

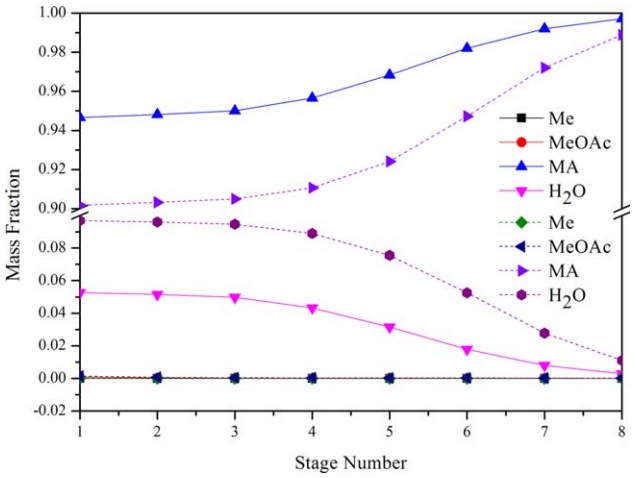

Figure 24. Composition distribution for Me-MeOAc-H_2O-MA quaternary system in the dehydration column.

[Color figure can be viewed in the online issue, which is available at wileyonlinelibrary.com.]

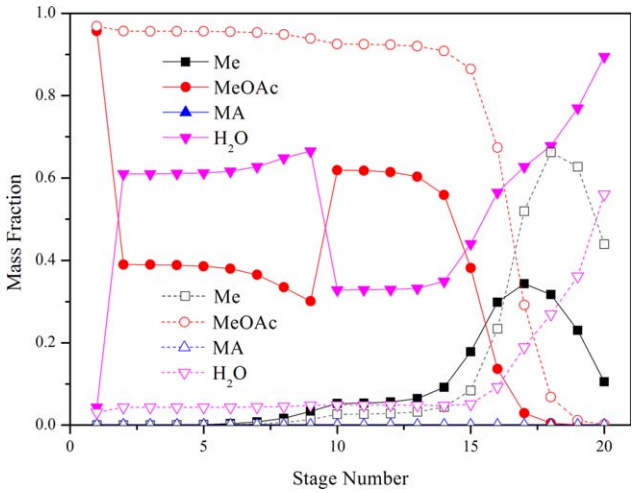

Figure 25. Composition distribution for Me-MeOAc-H_2O-MA quaternary system in the extraction column.

[Color figure can be viewed in the online issue, which is available at wileyonlinelibrary.com.]

composition distributions of the two columns are shown in Figures 23 and 24.

Conclusions

VLLE properties data were measured for binary and ternary systems containing H_2O, MA, MeOAc, and Me at temperatures ranging from 300 K to 373 K. The estimated VLLE compositions using the NRTL equation agreed well with the experimental data. The VLE data of MA-Me-H_2O ternary system was successfully reflected in tridimensional VLE phase diagrams. Meanwhile, the composition tetrahedron was constructed to intuitively present the LLE data of the quaternary system. The residue curve map of the ternary mixture MA-Me-H_2O showed that the Me-MA mixture could be separated using H_2O as extractant in the extraction column. Based on the thermodynamics and residue curve, two separation processes were designed and optimized. The high-purity products (99.9 wt % for MA product) and the lowest energy consumption were obtained by using decanter in a dehydration distillation column. In addition, we attempted to extend the separation approach to the quaternary system, which generated acceptable results. The separation technology has a guiding significance for MA production using acetic acid as the raw material.

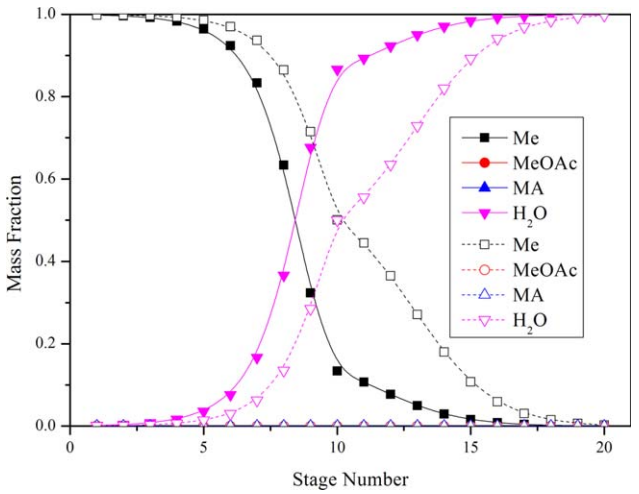

Figure 26. Composition distribution for Me-MeOAc-H_2O-MA quaternary system in the distillation column for Me recovery.

[Color figure can be viewed in the online issue, which is available at wileyonlinelibrary.com.]

Acknowledgment

The authors gratefully acknowledge the National Program on Key Basic Research Project (No. 2015CB251401), The National Natural Science Funds for Distinguished Young Scholar (No. 21425625) and The National Science Fund for Excellent Young Scholars (No. 21422607).

Literature Cited

1. Wang Y, Lang X, Zhao G, Chen H, Fan y, Yu L, Ma X, Zhu Z. Preparation of Cs-La-Sb/SiO 2 catalyst and its performance for the synthesis of methyl acrylate by aldol condensation. *RSC Adv*. 2015; 5(41):32826–32834.
2. Traa Y. Is a renaissance of coal imminent?—challenges for catalysis. *Chem Commun*. 2010;46(13):2175–2187.
3. Jo BY, Kum SS, Moon SH. Performance of WO_x-added Mo-V-Te-Nb-O catalysts in the partial oxidation of propane to acrylic acid. *Appl Catal A Gen*. 2010;378(1):76–82.
4. Amakawa K, Kolenko YV, Schlogl R, Trunschke A. The M1 phase of MoVTeNbO as a catalyst for olefin metathesis and isomerization. *ChemCatChem*. 2014;6(12):3338–3341.
5. Zhong Y, Wu Y, Zhu J, Chen K, Wu B, Ji L. Thermodynamics in separation for the ternary system 1,2-ethanediol + 1,2-propanediol + 2,3-butanediol. *Ind Eng Chem Res*. 2014;53:12143–12148.
6. Xu ZP, Chuang KT. Correlation of vapor-liquid equilibrium data for MeOAc-methanol-water-acetic acid mixtures. *Ind Eng Chem Res*. 1997;36(7):2866–2870.
7. Yang D, Li D, Yao HY, Zhang GL, Jiao TT, Li ZX, Li CS, Zhang SJ. Reaction of Formalin with Acetic Acid over Vanadium–Phosphorus Oxide Bifunctional Catalyst. *Ind Eng Chem Res*. 2015;54:6865–6873.
8. Zuo CC, Pan LS, Cao SS, Li CS, Zhang SJ. Catalysts, kinetics and reactive distillation for methyl acetate synthesis. *Ind Eng Chem Res*. 2014;53:10540–10548.
9. Debenedetti PG. Structure, dynamics and thermodynamics in complex systems: theoretical challenges and opportunities. *AIChE J*. 2005;51(9):2391–2395.
10. Bernatová S, Aim K, Wichterle I. Isothermal vapour-liquid equilibrium with chemical reaction in the quaternary water+ methanol+ acetic acid+ MeOAc system, and in five binary subsystems. *Fluid Phase Equilib*. 2006;247:96–101.
11. Arce A, Blanco A, Martinez-Ageitos J, Vidal I. LLE data for the system water + (methanol or ethanol) + n-amyl acetate. *Fluid Phase Equilib*. 1995;109:291–297.
12. Zhao S, Chen H, Chen X, Zhou J, Wang L. Liquid-liquid equilibrium of ternary and quaternary systems including MeOAc, benzene, toluene, and water at 283.2 K under atmosphere. *J Chem Eng Data*. 2010;55(11):5276–5279.
13. Genduso G, Amelio A, Luis P, Bruggen B, Vreysen, S. Separation of methanol-tetrahydrofuran mixtures by heteroazeotropic distillation and pervaporation. *AIChE J*. 2014;60(7):2584–2595.
14. Yang X, Dong HG, Grossmann IE. A framework for synthesizing the optimal separation process of azeotropic mixtures. *AIChE J*. 2012;58(5):1487–1502.
15. Wasylkiewicz SK, Sridhar LN, Doherty MF, Malone MF. global stability analysis and calculation of liquid-liquid equilibrium in multicomponent mixtures. *Ind Eng Chem Res*. 1996;35(4):1395–1408.
16. Haneda A, Seki T, Kodama D, Kato M. High-pressure phase equilibrium for ethylene + methanol at 278.15 K and 283.65 K. *J Chem Eng Data*. 2006;51(1):268–271.
17. Chai Q, Wan H, Wang L, Guan, G. Investigation on isobaric vapor-liquid equilibrium for water + acetic acid + sec-butyl acetate. *J Chem Eng Data*. 2014;59:1998–2003.
18. Agrawal R, Fidkowski ZT. Improved direct and indirect systems of columns for ternary distillation. *AIChE J*. 1998;44(4):823–830.

19. Li CS, Zhang XP, Zhang SJ, Suzuki K. Environmentally conscious design of chemical processes and products: multi-optimization method. *Chem Eng Res Des*. 2009;87(2):233–243.
20. Rodriguez-Donis I, Papp K, Lelkes Z, Gerbaud V, Joulia X. Column configurations of continuous heterogeneous extractive distillation. *AIChE J*. 2007;53(8):1982–1993.
21. Rooks RE, Julka V, Doherty MF, Malone MF. Structure of distillation regions for multicomponent azeotropic mixtures. *AIChE J*. 1998;44(6):1382–1391.
22. Cai J, Cui X, Zhang Y, Li R, Feng T. Vapor-liquid equilibrium and liquid-liquid equilibrium of MeOAc + methanol + 1-ethyl-3-methylimidazolium acetate. *J Chem Eng Data*. 2011;56(2):282–287.
23. Martin MC, Mato RB. Isobaric vapor-liquid equilibrium for methyl acetate + methanol + water at 101.3 kPa. *J Chem Eng Data*. 1995; 40(1):326–327.
24. Tu C, Wu Y, Liu T. Isobaric vapor-liquid equilibria of the methanol, methyl acetate and methyl acrylate system at atmosphereic pressure. *Fluid Phase Equilib*. 1997;135:97–108.
25. Li CS, Wozny G, Suzuki K. Design and Synthesis of separation process based on a hybrid method. *Asia-Pac J Chem Eng*. 2009;4(6):905–915.
26. Jiao TT, Zhuang XL, He HY, Zhao LH, Li CS, Chen HN, Zhang SJ. An ionic liquid extraction process for the separation of indole from wash oil. *Green Chem* 2015;17:3783–3790.
27. Güzel G, Xu X. Phase equilibria (LLE and VLE) of refining operations for enzymatic biodiesel production via quantum mechanical COSMO-RS method. *AIChE J*. 2012;58(11):3504–3516.
28. Li G, Asselin E, Li Z. Process simulation of sulfuric acid recovery by azeotropic distillation: vapor-liquid equilibria and thermodynamic modeling. *Ind Eng Chem Res*. 2014;53(29):11794–11804.
29. Reshtov. Azeotropic phenomenon in the five components mixture of Alcohol - Acrylate - H_2O - β ether propionate - Acrylic acid. *Zh. Prikl. Khim. (Leningrad)* 1988;61:(1):97–100.
30. Yee D, Simonetty J, Tassios D. Prediction of vapor-liquid equilibrium from ternary liquid-liquid equilibrium data. *Ind Eng Chem Process Des Dev*. 1983;22(1):123–129.
31. Renon H, Prausnitz JM. Local compositions in thermodynamic excess functions for liquid mixtures. *AIChE J*. 1968;14(1):135–144.
32. Liu H, Cui X, Zhang Y, Feng T, Yang Z. Isobaric vapor–liquid equilibrium of ethanenitrile + water + 1,2-ethanediol + 1-ethyl-3-methylimidazoliumchloride. *Fluid Phase Equilibr*. 2014; 378:13–20.
33. Topphoff M, Kiepe J, Gmehling J. Effects of lithium nitrate on the vapor-liquid equilibria of methyl acetate+ methanol and ethyl acetate+ ethanol. *J Chem Eng Data*.2001;46(5):1333–1337.
34. Kato R, Krummen M, Gmehling J. Measurement and correlation of vapor–liquid equilibria and excess enthalpies of binary systems containing ionic liquids and hydrocarbons. *Fluid Phase Equilibr*. 2004; 224(1):47–54.
35. Döker M, Gmehling J. Measurement and prediction of vapor–liquid equilibria of ternary systems containing ionic liquids. *Fluid Phase Equilibr*. 2005;227(2):255–266.
36. Anderson TF, Prausnitz JM. Application of the UNIQUAC equation to calculation of multicomponent phase equilibria. 1. Vapor-liquid equilibria. *Ind Eng Chem Process Des Dev*. 1978;17(4):552–561.
37. Yang C, Qian Y, Jiang Y, Zhang L. Liquid–liquid equilibria for the quaternary system methyl isobutyl ketone–water–phenol–hydroquinone. *Fluid Phase Equilibr*. 2007;258(1):73–77.
38. Ahmad SA, Tanwar, RS, Gupta RK, Khanna A. Interaction parameters for multi-component aromatic extraction with sulfolane. *Fluid Phase Equilibr*. 2004;220(2):189–198.
39. Vasquez VR, Whiting WB. Regression of binary interaction parameters for thermodynamic models using an inside-variance estimation method (IVEM). *Fluid Phase Equilibr*. 2000;170(2):235–253.

Manuscript received Feb. 24, 2015, and revision received June 10, 2015.